Sains Malaysiana 54(8)(2025): 2075-2086
http://doi.org/10.17576/jsm-2025-5408-16

Radiation Dose Study of LINAC Source around Healthy Organs in Cancer Examination using Farmer Chamber Ionization Detector

(Kajian Dos Sinaran Sumber LINAC di Sekitar Organ Sihat dalam Pemeriksaan Kanser menggunakan Pengesan Kebuk Pengionan Petani)

RAMACOS FARDELA[1,*], EGA SEPTRYAN CANDRA[1], DIAN MILVITA[1], DEDI MARDIANSYAH[1], RIDWAN[2] & FIQI DIYONA[3]

[1]*Department of Physics, Faculty of Mathematics and Natural Science, Universitas Andalas, Sumatera Barat, 25163, Indonesia*
[2]*Siemens Healthineers Company, Forchheim-91301, Germany*
[3]*Medical Physics, Radiotherapy Installation, Unand Hospital, Padang, 25176, Indonesia*

Received: 26 December 2024/Accepted: 23 June 2025

ABSTRACT

Cancer treatment using ionizing radiation is known to cause damage to healthy tissue around the target. Therefore, this study aimed to measure the dose in the area around the cancer target to ensure the amount received by the patient does not exceed the specified tolerance limit. Measurements were performed using a Farmer-type ionization chamber detector on a phantom slab. The variations in the field area used were 5 × 5 cm^2 and 10 × 10 cm^2 at depths of 1.5 cm, 4 cm, 6 cm, 8 cm, and 10 cm, as well as a distance of 3 cm, 5 cm, 7 cm, 10 cm, and 15 cm outside the radiation field. The dose value was measured based on the IAEA TRS No.398 protocol. The results showed that the percentage of the dose decreased below 10% at a distance of 5 cm for a field area of 5 × 5 cm^2. Meanwhile, for a field area of 10 × 10 cm^2, the percentage of the dose decreased below 10% after passing a distance of 7 cm from the edge of the radiation field. Based on the results, the percentage of the measured dose was greater for the enlarged depth. Areas outside the cancer target still receive unneeded radiation doses. The value of the dose received depends on the energy used, the size of the field, and the distance from the edge of the field.

Keywords: Cancer; depth; dose; edge distance; LINAC

ABSTRAK

Rawatan kanser menggunakan sinaran pengionan diketahui boleh menyebabkan kerosakan pada tisu sihat di sekeliling sasaran. Justeru, penyelidikan ini bertujuan untuk mengukur dos di kawasan sekitar sasaran kanser bagi memastikan jumlah yang diterima pesakit tidak melebihi had toleransi yang ditetapkan. Pengukuran dilakukan menggunakan pengesan kebuk pengionan jenis Petani pada papak fantom. Variasi luas lapangan yang digunakan ialah 5 × 5 cm^2 dan 10 × 10 cm^2 pada kedalaman 1.5 cm, 4 cm, 6 cm, 8 cm dan 10 cm serta jarak 3 cm, 5 cm, 7 cm, 10 cm dan 15 cm di luar medan sinaran. Nilai dos diukur berdasarkan protokol IAEA TRS No. 398. Keputusan menunjukkan bahawa peratusan dos menurun di bawah 10% pada jarak 5 cm untuk kawasan medan seluas 5 × 5 cm^2. Manakala, bagi kawasan medan seluas 10 × 10 cm^2, peratusan dos menurun di bawah 10% selepas melepasi jarak 7 cm dari tepi medan sinaran. Berdasarkan keputusan, peratusan dos yang diukur adalah lebih besar untuk kedalaman yang diperbesarkan. Kawasan di luar sasaran kanser masih menerima dos sinaran yang tidak diperlukan. Nilai dos yang diterima bergantung pada tenaga yang digunakan, saiz medan dan jarak dari tepi medan.

Kata kunci: Dos; jarak tepi; kanser; kedalaman; LINAC

INTRODUCTION

Cancer is among the most significant global health problems affecting lives, and treatment includes various methods, including radiotherapy (Khan 2014; Mohan 2022). The method uses high radiation to destroy cancer cells or inhibit growth. It is crucial in cancer management as primary, additional, and palliative therapy (Bosse et al. 2020). The treatment can be used for various purposes, depending on the kind and stage of cancer. For example, radiotherapy is often used to shrink tumors before surgery (neoadjuvant therapy), kill remaining cancer cells after surgery (adjuvant therapy), or relieve symptoms that cannot be cured (palliative therapy). Various methods are used such as external radiotherapy, where radiation is directed from outside the body, or brachytherapy, where the radiation source is placed directly in or near the tumor (Bresolin et al. 2017; Sung et al. 2017; Wang & Tepper 2021).

Linear Accelerator (LINAC) is a prominent radiotherapy modality in cancer treatment, which produces

photon or electron radiation directed precisely to the target area in the body (De Saint-Hubert et al. 2022; Naji et al. 2022). This system allows for precise radiation dose settings and can be adjusted to the shape and size of the tumor, as well as the position and condition of the patient (Momeni et al. 2023). The ability to deliver high radiation doses locally, while reducing the impact on healthy tissue, makes LINAC the primary choice in treating various types of cancer, including breast, prostate, and lung (Antolak & Rosen 1999).

During therapy planning using LINAC, it is also important to consider the radiation dose received by tissues outside the radiation field, or peripheral dose (Burnet et al. 2004; Liu et al. 2018). Specifically, this dose refers to healthy tissues indirectly exposed to radiation from the therapy source. Radiation dose outside the radiation field can occur due to various factors, including scattering from the main field, secondary radiation, and leakage from radiotherapy devices such as LINAC (Huang et al. 2009). Although this dose is usually significantly lower than the amount received by the target area, repeated or significant exposure can pose health risks, such as the potential for secondary cancers and long-term tissue damage (Matuszak et al. 2022).

The Percentage Depth Dose (PDD) curve is an important tool for describing the radiation dose distribution in body tissues at various depths relative to the skin surface. It provides information about the decrease in radiation dose as the depth from the skin surface increases (Licona, Figueroa-Medina & Gamboa-deBuen 2017). This data is important for designing and setting the appropriate dose in the tumor target area and identifying and managing the radiation dose received by the surrounding healthy tissue (Howell et al. 2010; Kry et al. 2006; Li, Ma & Salhani 1997). For example, the PDD curve helps determine the amount of radiation the healthy tissue receives below the target area. It plays a role in calculating the effective dose to achieve optimal therapeutic results.

The dose outside the radiation field, which includes those reaching areas outside the central radiation zone, is usually lower than the amount received by the direct target. However, long-term or cumulative exposure can cause significant side effects on healthy tissues and increase the risk of secondary cancers (Dinh & Nowak 2021; Licona, Figueroa-Medina & Gamboa-deBuen 2017). The results will provide valuable data to improve treatment planning, enhance patient safety, as well as inform future developments in LINAC technology and shielding designs. By better understanding the actual radiation exposure to healthy tissues, clinicians can make more informed decisions about treatment parameters and potentially reduce the risk of complications in cancer patients (Taylor & Kron 2011).

Studies have shown that the radiation dose outside the field can vary depending on several factors, including the radiotherapy method used, the type of radiation applied, and the design of the radiotherapy device (Garrett et al. 2021; Podgorsak 2005). Various dosimetry protocols recommend the cylindrical Farmer-type ionization chamber for accurately measuring radiation doses in radiotherapy beams. The precision, reproducibility, and minimal energy dependence make these detectors ideal for absolute dose measurements in high-energy photon beams (Marín et al. 2015; Wiezorek et al. 2009). Furthermore, recent advancements in Farmer-type chamber design have improved the reliability. Modern chambers are characterized by minimal leakage (typically within 0.08%), excellent long-term stability (within 0.07%), and limited stem effect (within 0.3%). These characteristics make the Farmer chamber appropriate for investigating out-of-field doses in LINAC-based radiotherapy (Raj et al. 2022; Saminathan et al. 2016). In this study, peripheral dose measurements were carried out to ensure that the healthy tissue around the cancer target did not exceed the dose volume given (Balasubramanian et al. 2006; Park et al. 2012).

METHODS

The Clinac CX type LINAC was used as a radiation source in radiotherapy treatment using photon and electron beams, while the energy source was a 6 MV photon beam. The measurement detector used was a farmer-type ionization chamber detector that captured the output of the photon beam emitted from the LINAC and a phantom slab made of water-equivalent polystyrene (RW3) used as a substitute for the human body in irradiation (Balasubramanian et al. 2006). The material composition of the phantom includes 98% Polystyrene (C_8H_8) and 2.1 g/cm^3 TiO^2 (TRS 2000). In contrast to previous studies, where water phantoms were used to measure peripheral doses, the RW3 phantom was used to determine the peripheral dose obtained. The use of RW3 phantoms provides several advantages over water phantoms in measuring out-of-field dose in radiotherapy. The RW3 phantom has an anthropomorphic design and composite material that resembles human tissue, allowing it to mimic the dose distribution in organs and tissues more realistically than the homogeneous water phantom. It is commonly used for radiotherapy QA due to the water-equivalent density. In addition, RW3 allows detectors to be placed at various positions and depths according to clinical needs, resulting in more accurate and representative dose mapping in off-target areas. Another advantage is cost-efficiency and ease of operation, as RW3 can be produced locally at a lower cost and does not require a complex support system compared to water phantoms (Gargett, Briggs & Booth 2020; Hong, Lee & Cho 2015). This study was conducted on a small field area of 5 × 5 cm^2 and a reference field area of 10 × 10 cm^2. The radiation beam was a 6 MV photon beam with a smaller scattering rate than a 10 MV photon beam. Moreover, 6 MV photons are frequently used in UNAND Hospital radiotherapy treatment. This study did not measure the peripheral dose for 10 MV photon beams because it can cause the equipment to become radioactive and endanger medical personnel and patients in the room (Swanpalmer 2024).

The peripheral dose measurement scheme is shown in Figure 1. The ionization chamber detector, IBA CC13, was connected to the electrometer using a numbered cable as a connector. The detector was placed on the phantom to read the radiation dose received on the beam's central axis (CAX) or in the peripheral area. The dose absorbed by the detector was then read on the electrometer. To obtain the percentage of the peripheral dose, Equation (1) was used.

$$PD = \frac{M}{M_{CAX}} x\ 100\% \quad (1)$$

where *PD* is the peripheral dose; *M* is the charge value read at the measurement point; and M_{cax} is the charge value read on the central axis of the beam (CAX).

A 6 MV photon beam was radiated on a field area of 5 × 5 cm^2 and 10 × 10 cm^2; the depths used were d_{max}, 4 cm, 6 cm, 8 cm, and 10 cm. The measurement points used were the beam's central axis or CAX, a distance of 3 cm, 5 cm, 7 cm, 10 cm, and 15 cm from the edge of the radiation field. The measurements carried out can be visualized in the form of images shown in Figure 2.

Each phantom beam measured 1 cm in size, and the detector was positioned on the phantom at the desired depth. Based on the detector measurement results, the relationship between the peripheral dose and the depth, as well as the field size and distance from the edge of the irradiation field, was obtained.

After the measurement, the results were multiplied by a correction factor based on the TRS No. 398 standard to improve the accuracy of the value and conformity with the reference standard. Pressure and temperature correction factors were measured against the reference state. This correction factor was calculated using Equation (2) (International Atomic Energy Agency 2008).

$$K_{TP} = \frac{273{,}2 + T}{273{,}2 + T_0} \times \frac{P_0}{P} \quad (2)$$

where T is the temperature when the measurement was made (°C) and *P* is the air pressure during measurement (kPa). Meanwhile, T_0 and P_0 are the reference temperature and pressure in the ionization chamber detector calibration certificate, respectively.

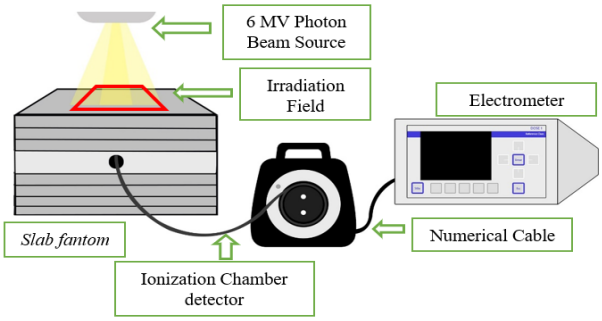

FIGURE 1. Study material arrangement

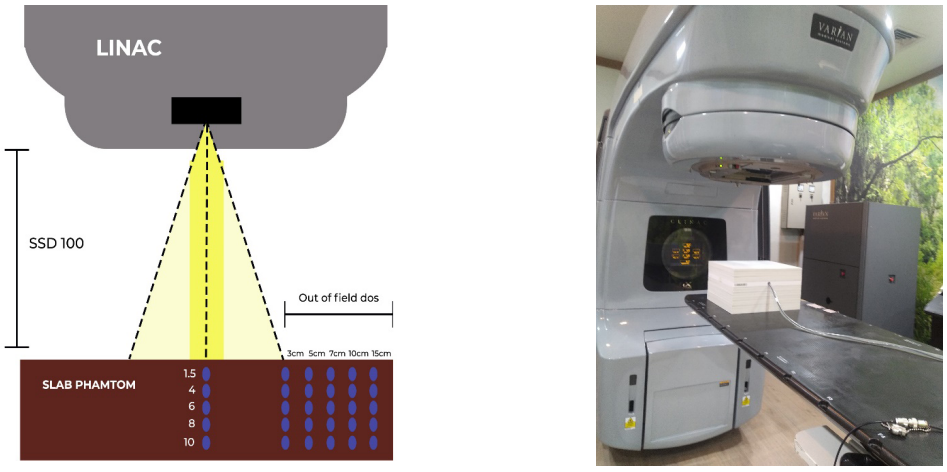

(a) (b)

FIGURE 2. Peripheral dose measurement scheme

The electrometer correction factor is 1 when the ionization chamber detector is calibrated with the electrometer. The polarization correction factor represents the response of the ionization chamber detector to the polarity effects. The polarization correction factor was calculated using Equation (3).

$$K_{pol} = \frac{|M_+|+|M_-|}{2M} \quad (3)$$

where M is the charge reading at the polarity used routinely (nC); M_+ is the charge reading at the Positive polarity (nC); and M_- is the reading at the negative polarity (nC).

Ion recombination was performed to calculate the detector response correction factor for incomplete charge collection during ionization in air. This correction factor was calculated using Equation (4).

$$k_S = a_0 + a_1 \left(\frac{M_1}{M_2}\right) + a_2 \left(\frac{M_1}{M_2}\right)^2 \quad (4)$$

where a_0, a_1, and a2 are quadratic coefficients to calculate the KS value using the two-voltage method based on (Table 9, TRS No. 398, IAEA). M_1 reading is the measurement for the commonly used voltage, and M_2 reading is the measurement for the reference voltage.

The detector response correction factor in beam quality was used as detector calibration (Co-60) to the photon beam quality according to Table 6. III TRS No. 398 IAEA. The results of this correction factor reading were calculated using Equation (5).

$$M_Q = M.\ k_{tp}.k_{elec}.k_{pol}.k_s \quad (5)$$

where M is the result of the charge reading at the time of measurement (nC/MU); k_{tp} is the pressure and temperature correction factor for the reference condition; k_{elec} is the electrometer calibration factor with a value of 1; k_{pol} is the ionization detector response correction factor for the polarity effect on the detector; k_s is the ionization chamber detector response correction factor for the incomplete collection of charges during ionization in air (Sánchez-Nieto et al. 2020).

RESULTS AND DISCUSSION

PERCENTAGE DEPTH DOSE MEASUREMENT OF THE 6 MV PHOTON BEAM

Figure 3 shows the relationship between depth and PDD value in the 6 MV photon beam. The deeper the target depth in the phantom, the greater the PDD value obtained until the maximum depth was reached (Z_{max}). The maximum dose value (D_{max}) was located at Z_{max}, where the maximum depth in the PDD measurement was 1.5 cm. This value follows the theory stating that Z_{max} in the 6 MV photon beam is at a depth of 1.5 cm. After passing the maximum depth, the radiation dose decreased as the depth of the phantom increased (Connell & Hellman 2009).

Figure 3 also shows PDD values appropriate to the theory in Podgorsak (2005), stating that the dose value will increase as the depth of the phantom increases until the maximum depth is reached and then decreases due to the influence of photon attenuation. In this context, photon attenuation occurs due to a decrease in the number of ions caused by reduced electron production. The energy and the beam's size influenced the dose's maximum depth. The nominal value for the maximum depth of the shallow X-ray beam and Orthovoltage was 0, C0-60 reached 0.5 cm, and the photon beam up to 25 MV reached 5 cm (DeWerd & Kissick 2013).

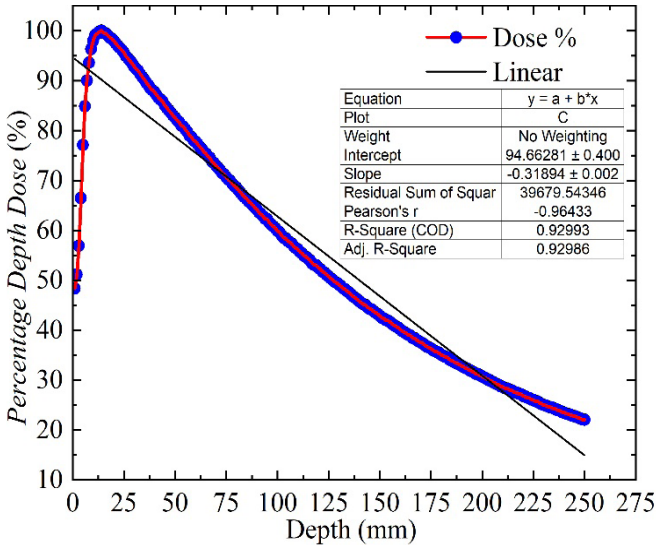

FIGURE 3. PDD curve of 6 MV photon beam measurement results

PERIPHERAL DOSE MEASUREMENT BASED ON EDGE-OF-FIELD DISTANCE

In this study, the depth is symbolized by *d*, and the distance from the edge of the field is represented by *x*. The peripheral dose measurement results based on the edge of the field distance using a Farmer-type ionization chamber detector are presented in Figures 4 and 5.

Figure 4 shows that in the field area 5 × 5 cm^2, the measurement point is 3 cm outside the radiation field, and the measured dose is relatively large with a percentage of around 30-35%. This can be caused by the measurement area being very close to the radiation field, allowing the detector to absorb a large scattered dose. When the measurement point was at a distance of 5 cm from outside the radiation field, the measured peripheral dose decreased sharply to a percentage below 5%, which was 2.2-3.8%. At a distance of 7 cm, the percentage of the peripheral dose was at 1.2 - 1.9%, and at a distance of 10 cm, the percentage of the dose was in the range of 0.6 - 0.9%. The percentage of dose continued to decrease until, finally, at a distance of 15 outside the radiation field, reaching 0.3-0.4%.

Physically, radiation intensity decreases following the inverse square law, hence, the further away from the source or the edge of the field, the smaller the dose received. Scattering radiation resulting from the interaction of photons with patient tissues and radiotherapy device components will lose energy and intensity as the distance from the edge of the field increases. Therefore, organs located farther from the boundary of the irradiation field receive a significantly lower dose than those located closer (Sánchez-Nieto et al. 2020).

As shown in Figure 5, the percentage dose value on the field area 10 × 10 cm^2 had a greater value compared to 5 × 5 cm^2. At a distance of 3 cm, the percentage of peripheral dose measured by the ionization chamber detector reached 95-100%. When the measurement was carried out at a point 5 cm outside the irradiation field, the percentage of the measured dose was 50-54%. The percentage of the measured peripheral dose only decreased to below 10% at a distance of 7 cm outside the irradiation field, reaching 4.7-8%. At a distance of 10 cm outside the irradiation field, the percentage of the dose obtained was 2.2-3.4%. The dose significantly reduced when the measurement distance from the edge of the field increased. At a distance of 15 cm, the percentage of the measured dose was between 0.8% and 1.1%.

Figures 4 and 5 show that the peripheral dose value decreased as the distance from the edge of the field increased. This can be caused by the presence of a *penumbra* region (Abdelaal, Attalla & Elshemey 2017; Inayat et al. 2019). *Penumbra* is a term used to define the area at the edge of the radiation beam. The *penumbra* dose decreases rapidly as a function of the distance from the beam's central axis. The effect is divided into three parts. The first is the transmission *penumbra* formed by the dose transmitted by the collimator tip (Inayat et al. 2019; Sung et al. 2017). The second effect is the geometric *penumbra*, which appears because the photon source is limited. Consequently, some sources are blocked near the edge of the field. Factors that influence the presence of a geometric *penumbra* are source size, SSD, field size, and the distance from the source to the collimator (Lam, Muthuswamy & Ten Haken 1996). The radiological *penumbra* effect is caused by the biological effect of electrons moving from their original place and storing energy elsewhere. The measurement results were consistent with previous studies stating that the further the measurement point, the lower the contribution of primary photons, where the radiation intensity decreases by the square of the distance from the source (Howell et al. 2010; Lam, Muthuswamy & Ten Haken 1996). Aside from the presence of *penumbra*, the characteristics of the photon radiation beam can also affect the magnitude of the measured dose value outside the irradiation field. The size of the radiation beam is one factor affecting the magnitude of the measured radiation dose value. The larger the radiation beam, the greater the scattering (Oancea et al. 2023; Zhu & Biarngard 1994).

The large percentage of dose on the field area 10 × 10 cm^2 compared to 5 × 5 cm^2 was caused by the contribution of secondary doses on small fields, which tended to be larger than the primary dose. Therefore, the radiation dose on the edge of the field with a field area 5 × 5 cm^2 was smaller. In small fields, scattered radiation is more dominant, and there is a greater risk of leakage from beam formation. The high dose value measured around the edge of the field can be caused by several factors, including the scattered dose on the gantry, the backscatter factor from the phantom, or the scattered dose on the collimator (Mazonakis & Damilakis 2021; Zhu & Biarngard 1994).

PERIPHERAL DOSE MEASUREMENT BASED ON DEPTH

The peripheral dose measurement results based on depth were plotted into a graph as shown in Figures 6 and 7. Based on Figure 6, at a depth of 1.5 cm, the percentage of the peripheral dose is in the range of 0.48-31.46%; at a depth of 4 cm, the percentage of the peripheral dose has increased to 0.39-30.15%; at a depth of 6 cm, the percentage of peripheral dose obtained is in the range of 0.41-31.2%, at a depth of 8 cm the percentage of the peripheral dose is 0.43-32.5%, and at a depth of 10 cm the percentage of peripheral dose obtained is in the range of 0.46-35.1%.

Based on Figure 7, at a depth of 1.5 cm, the percentage of the peripheral dose is in the range of 0.82-99.8%; at a depth of 4 cm, the percentage of the peripheral dose has increased to 0.83-99.4%; at a depth of 6 cm, the percentage of peripheral dose obtained is in the range of 0.9-98.8%, at a depth of 8 cm, the percentage of the peripheral dose is 1-98.5%, and at a depth of 10 cm the percentage of peripheral dose obtained is in the range of 1.-98.2%.

At shallow depths (1-2 cm), laterally scattered low-energy (0.2-0.6 MeV) Compton electrons dominate the out-of-field dose. As the tissue deepens (>3 cm), the contribution of photon scattering (bremsstrahlung)

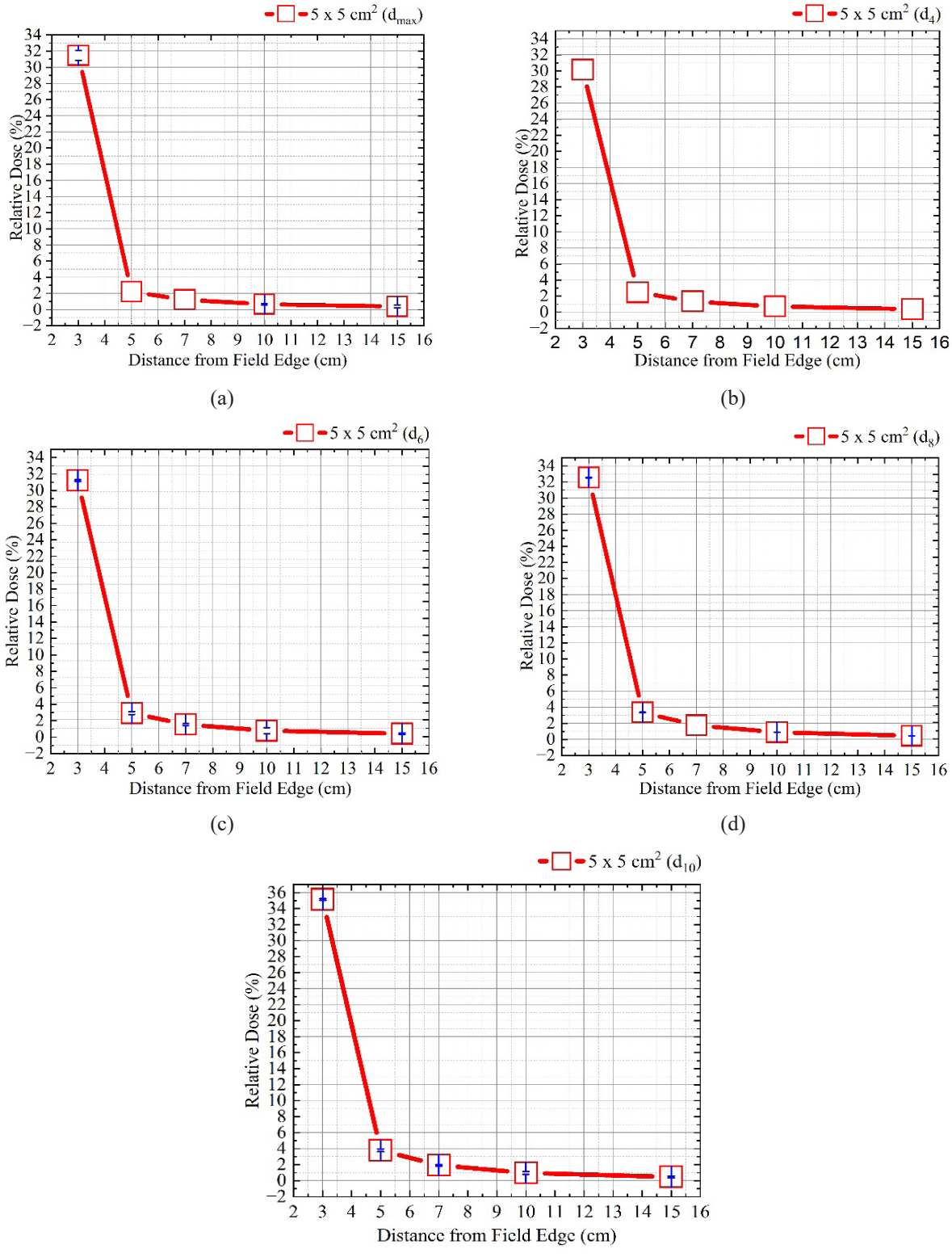

FIGURE 4. Percentage of peripheral dose based on field edge distance using a Farmer-type ionization chamber for a field area of 5 × 5 cm^2 (a) d_{max}, (b) d_4, (c) d_6, (d) d_8, and (e) d_{10}

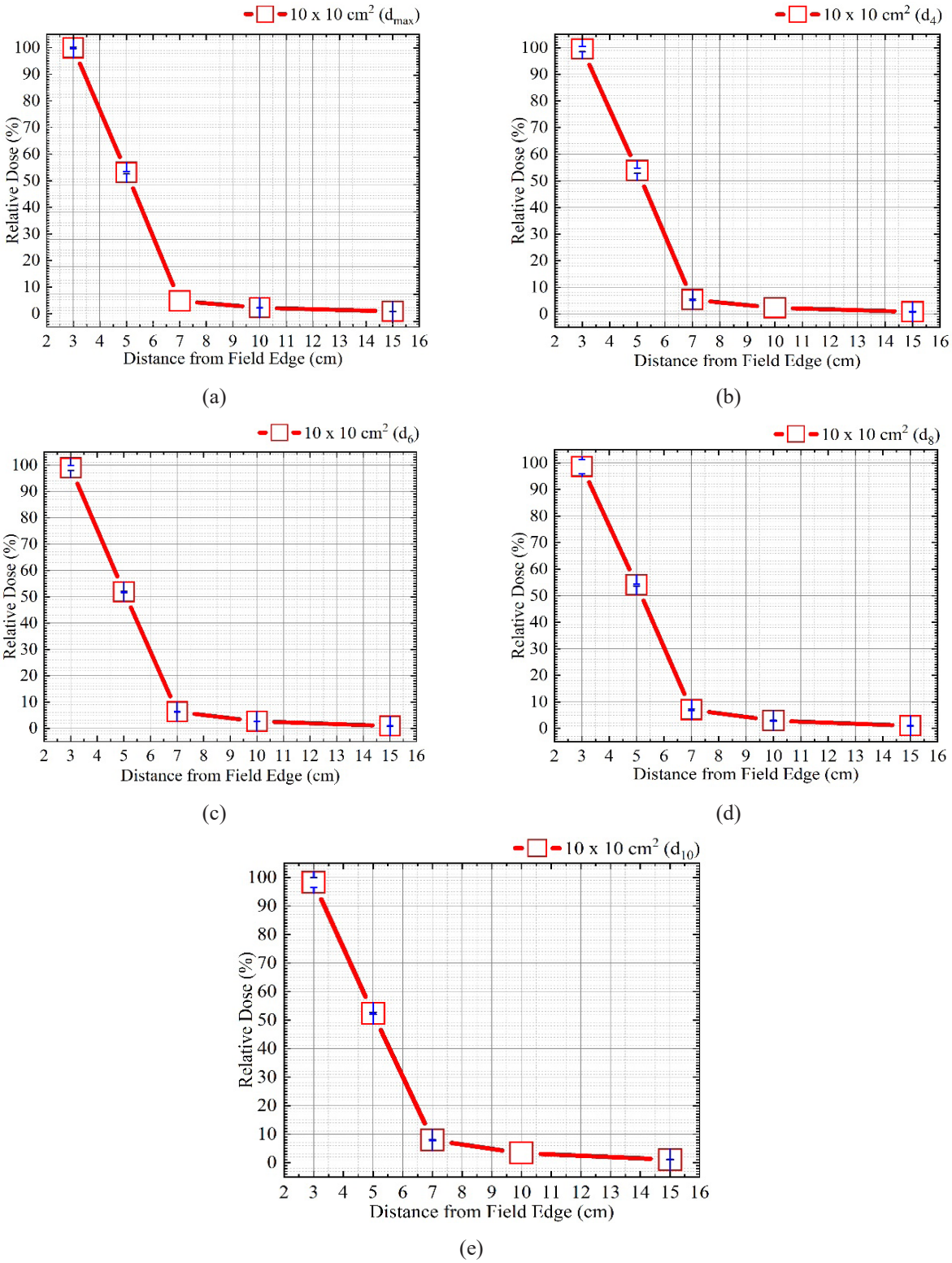

FIGURE 5. Percentage of peripheral dose based on field edge distance using a Farmer-type ionization chamber for a field area of 10 × 10 cm^2 (a) d_{max}, (b) d_4, (c) d_6, (d) d_8, and (e) d_{10}

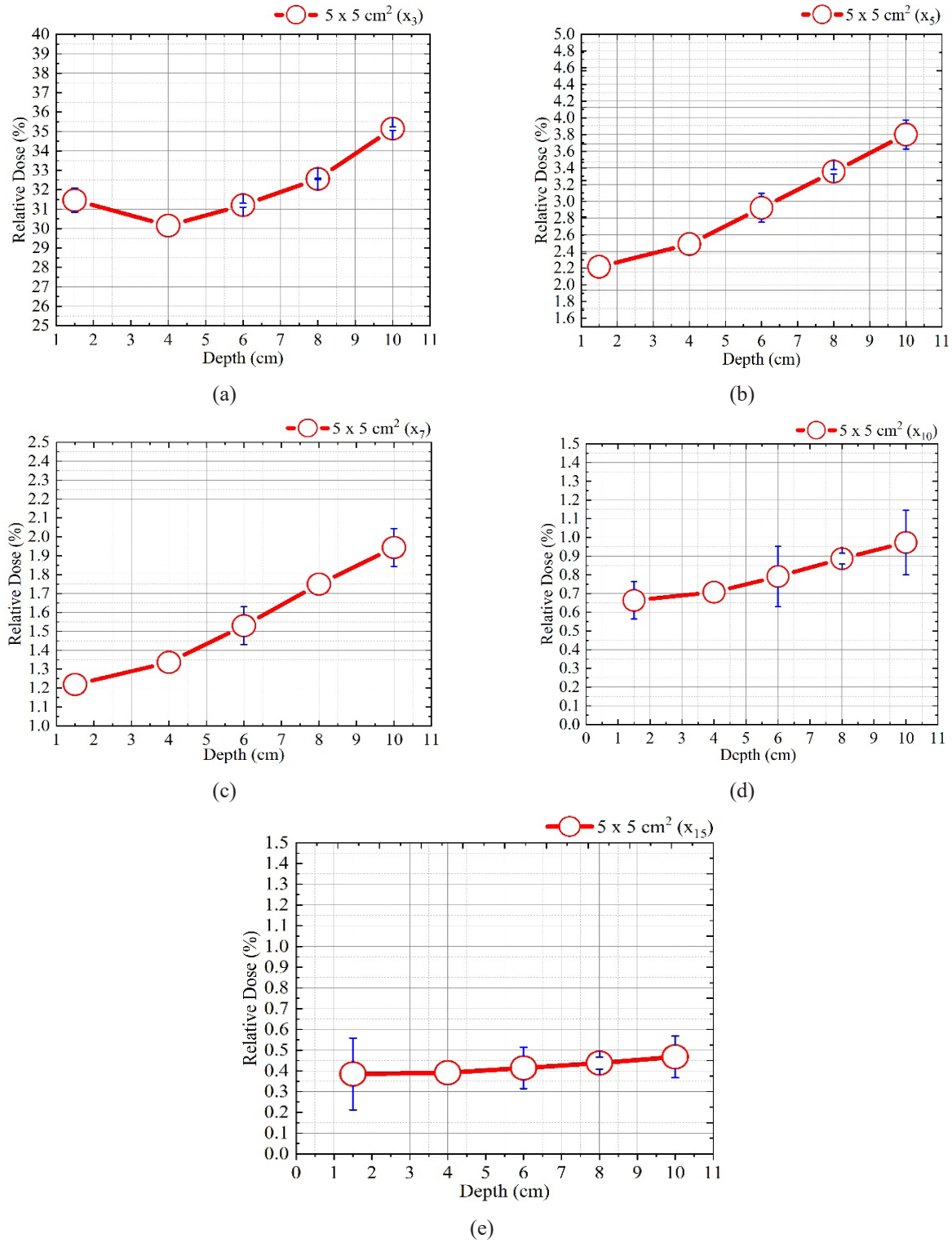

FIGURE 6. Percentage of peripheral dose to depth using a Farmer-type ionization chamber for a field area of 5 × 5 cm² (a) x_3, (b) x_5, (c) x_7, (d) x_{10}, and (e) x_{15}

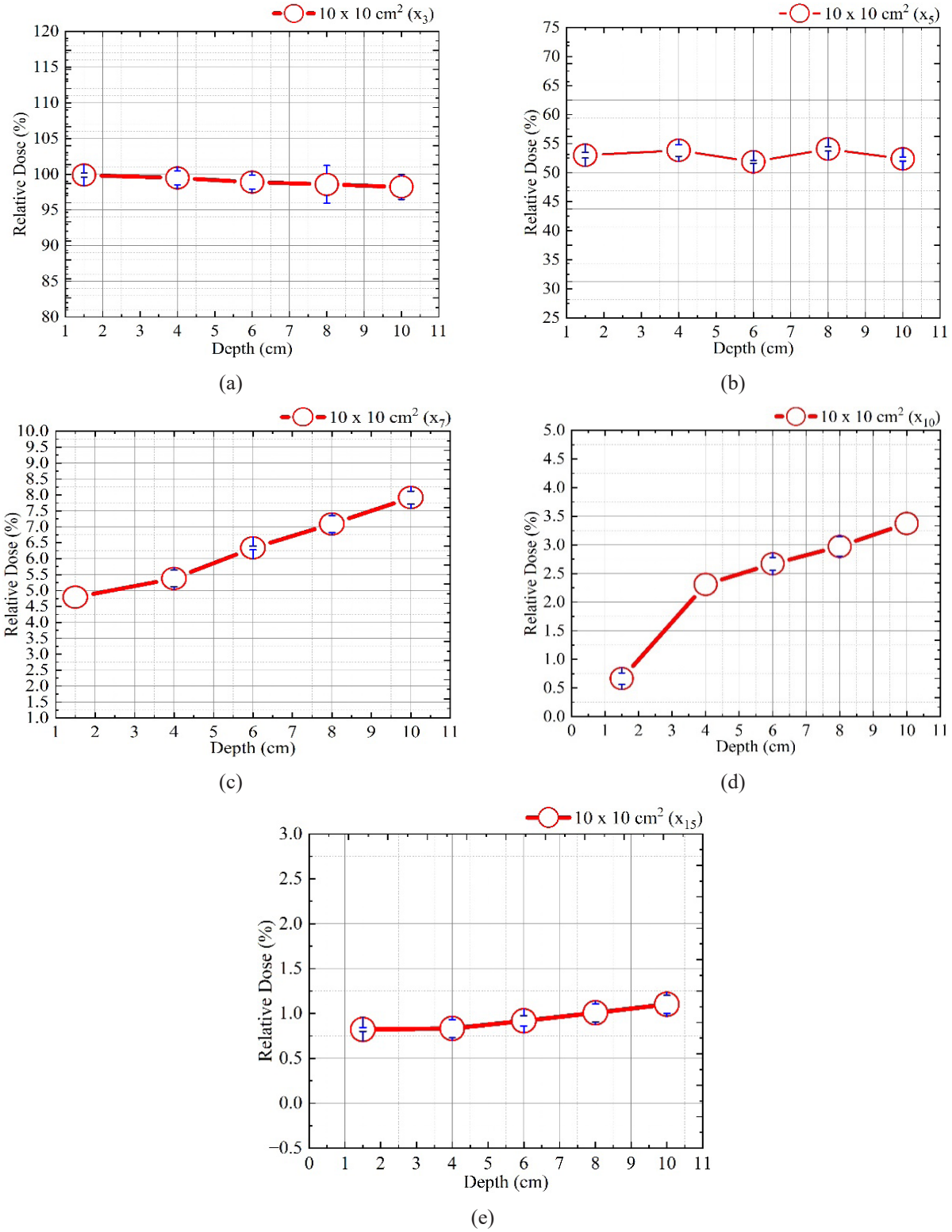

FIGURE 7. Percentage of peripheral dose to depth using a Farmer-type ionization chamber for a field area of 10 × 10 cm² (a) x_3, (b) x_5, (c) x_7, (d) x_{10}, and (e) x_{15}

increases due to multiple scattering, leading to a more homogeneous dose distribution (Matuszak et al. 2022; Pazzaglia et al. 2022). Based on the depth of the peripheral dose value as shown in Figures 6 and 7, the peripheral dose increased with greater depth. The increase in dose value was related to the interaction of radiation with matter. When radiation interacts with the body, some of the radiation given to the tissue around the tumor tends to be higher than the dose received by the tumor. This is because the radiation given will be scattered in various directions. The scattering causes the dose on the surface to be lower compared to a certain depth. In addition to being caused by radiation scattering, the increase in dose at each higher depth can be caused by the absorption factor (Mohsin et al. 2014). The deeper the radiation penetrates the tissue, the more energy is absorbed. This causes the dose on the surface to be lower compared to a certain depth. The measurement results obtained for the field area 10 × 10 cm^2 were greater than those for 5 × 5 cm^2. This was because a larger field area would produce greater photon scattering. Therefore, the larger the field area used, the greater the scattering at a greater dose (Abdelaal, Attalla & Elshemey 2020).

CONCLUSION

In conclusion, the peripheral dose value decreased as the measurement distance from the edge of the radiation field increased, and then reduced when the depth increased. Experimental studies with ionization detectors show that empirical measurements are still required to validate out-of-field doses, especially in the region <5% of the total amount of medically recommended radiation. In the out-of-field dose measurement for the 5 × 5 cm^2 field area, the dose value decreased by more than 10% when the measurement point was 5 cm from the edge of the irradiation field. For the 10 × 10 cm^2 field area, the dose value only decreased at a distance of 7 cm from the edge of the irradiation field. The peripheral dose value was influenced by the presence of a *penumbra* area around the target and the material interaction with the radiation beam, which could affect the radiation dose value for each depth and distance of the edge. Based on the results, treatment can be optimally organized by considering the radiation dose received in healthy tissues around the target area, including measurements using different energies for photons and electrons, as well as adding cancer types to determine the peripheral dose specifically in some instances.

ACKNOWLEDGEMENTS

We are grateful to the Directorate of Research, Technology, and Community Service, Directorate General of Higher Education, Research and Technology, Ministry of Education, Culture, Research and Technology for funding this study through Fundamental Research – Regular with contract number: 041/E5/PG.02.00.PL/2024.

REFERENCES

Abdelaal, A.M., Attalla, E.M. & Elshemey, W.M. 2020. Estimation of out-of-field dose variation using Markus ionization chamber detector. *SciMedicine Journal* 2(1): 8-15. https://doi.org/10.28991/scimedj-2020-0201-2

Abdelaal, A.M., Attalla, E.M. & Elshemey, W.M. 2017. Dose estimation outside radiation field using Pinpoint and Semiflex ionization chamber detectors. *Radiation Physics and Chemistry* 139: 120-125. https://doi.org/10.1016/j.radphyschem.2017.04.006

Antolak, J.A. & Rosen, I.I. 1999. Planning target volumes for radiotherapy: How much margin is needed? *International Journal of Radiation Oncology Biology Physics* 44(5): 1165-1170. https://doi.org/10.1016/S0360-3016(99)00117-0

Balasubramanian, R., Sellakumar, P., Bilimagga, R.S., Supe, S.S. & Sankar, B.N. 2006. Measurements of peripheral dose for multileaf collimator based linear accelerator. *Reports of Practical Oncology and Radiotherapy* 11(6): 281-285. https://doi.org/10.1016/S1507-1367(06)71073-2

Bosse, C., Narayanasamy, G., Saenz, D., Myers, P., Kirby, N., Rasmussen, K., Mavroidis, P., Papanikolaou, N. & Stathakis, S. 2020. Dose calculation comparisons between three modern treatment planning systems. *Journal of Medical Physics* 45(3): 143-147. https://doi.org/10.4103/jmp.JMP_111_19

Bresolin, A., Bonfantini, F., Stucchi, C.G., Mongioj, V., Carrara, M. & Pignoli, E. 2017. Study of the ionization chamber response to flattening-filter-free photon beams. *Radiation Measurements* 97: 47-53. https://doi.org/10.1016/j.radmeas.2016.12.011

Burnet, N.G., Thomas, S.J., Burton, K.E. & Jefferies, S.J. 2004. Defining the tumour and target volumes for radiotherapy. *Cancer Imaging* 4(2): 153-161. https://doi.org/10.1102/1470-7330.2004.0054

Connell, P.P. & Hellman, S. 2009. Advances in radiotherapy and implications for the next century: A historical perspective. *Cancer Research* 69(2): 383-392. https://doi.org/10.1158/0008-5472.CAN-07-6871

De Saint-Hubert, M., Suesselbeck, F., Vasi, F., Stuckmann, F., Rodriguez, M., Dabin, J., Timmermann, B., Thierry-Chef, I., Schneider, U. & Brualla, L. 2022. Experimental validation of an analytical program and a Monte Carlo simulation for the computation of the far out-of-field dose in external beam photon therapy applied to pediatric patients. *Frontiers in Oncology* 12: 882506. https://doi.org/10.3389/fonc.2022.882506

DeWerd, L.A. & Kissick, M. 2013. *The Phantoms of Medical and Health Physics: Devices for Research and Development*. New York: Springer.

Dinh, C.N. & Nowak, J. 2021. Natural radioactivity in thermal waters: A case study from poland. *Energies* 14(3): 541. https://doi.org/10.3390/en14030541

Gargett, M.A., Briggs, A.R. & Booth, J.T. 2020. Water equivalence of a solid phantom material for radiation dosimetry applications. *Physics and Imaging in Radiation Oncology* 14: 43-47. https://doi.org/10.1016/j.phro.2020.05.003

Garrett, L., Hardcastle, N., Yeo, A., Lonski, P., Franich, R. & Kron, T. 2021. Out-of-field dose in stereotactic radiotherapy for paediatric patients. *Physics and Imaging in Radiation Oncology* 19: 1-5. https://doi.org/10.1016/j.phro.2021.05.006

Hong, J.W., Lee, H.K. & Cho, J.H. 2015. Comparison of the photon charge between water and solid phantom depending on depth. *International Journal of Radiation Research* 13(3): 229-234.

Howell, R.M., Scarboro, S.B., Kry, S.F. & Yaldo, D.Z. 2010. Accuracy of out-of-field dose calculations by a commercial treatment planning system. *Physics in Medicine and Biology* 55(23): 6999-7008. https://doi.org/10.1088/0031-9155/55/23/S03

Huang, Y.J., Kuo, T.C., Chen, C.Y., Chang, C.H., Wu, P.C. & Wu, T.H. 2009. The design and implementation of a solar tracking generating power system. *Engineering Letters* 17: 4.

Inayat, A., Nassef, A.M., Rezk, H., Sayed, E.T., Abdelkareem, M.A. & Olabi, A.G. 2019. Fuzzy modeling and parameters optimization for the enhancement of biodiesel production from waste frying oil over montmorillonite clay K-30. *Science of the Total Environment* 666: 821-827. https://doi.org/10.1016/j.scitotenv.2019.02.321

International Atomic Energy Agency. 2008. IAEA Technical Report Series. *European Journal of Nuclear Medicine and Molecular Imaging* 35(5): 1030-1031. https://doi.org/10.1007/s00259-008-0767-4

Khan, F.M. 2014. *The Physics of Radiation Therapy* (5 ed.). Lippincott Williams & Wilkins.

Kry, S.F., Titt, U., Pönisch, F., Followill, D., Vassiliev, O.N., White, R.A., Mohan, R. & Salehpour, M. 2006. A Monte Carlo model for calculating out-of-field dose from a varian 6 MV beam. *Medical Physics* 33(11): 4405-4413. https://doi.org/10.1118/1.2360013

Lam, K.L., Muthuswamy, M.S. & Ten Haken, R.K. 1996. Flattening-filter-based empirical methods to parametrize the head scatter factor. *Medical Physics* 23(3): 343-352. https://doi.org/10.1118/1.597798

Li, X.A., Ma, C.M. & Salhani, D. 1997. Measurement of percentage depth dose and lateral beam profile for kilovoltage x-ray therapy beams. *Physics in Medicine and Biology* 42(12): 2561-2568. https://doi.org/10.1088/0031-9155/42/12/019

Licona, I., Figueroa-Medina, E. & Gamboa-deBuen, I. 2017. Dose distributions and percentage depth dose measurements for a total skin electron therapy. *Radiation Measurements* 106: 365-372. https://doi.org/10.1016/j.radmeas.2016.12.002

Liu, Q., Liang, J., Zhou, D., Krauss, D.J., Chen, P.Y. & Yan, D. 2018. Dosimetric evaluation of incorporating patient geometric variations into adaptive plan optimization through probabilistic treatment planning in head and neck cancers. *International Journal of Radiation Oncology Biology Physics* 101(4): 985-997. https://doi.org/10.1016/j.ijrobp.2018.03.062

Marín, A., Martín, M., Liñán, O., Alvarenga, F., López, M., Fernández, L., Büchser, D. & Cerezo, L. 2015. Bystander effects and radiotherapy. *Reports of Practical Oncology and Radiotherapy* 20(1): 12-21. https://doi.org/10.1016/j.rpor.2014.08.004

Matuszak, N., Kruszyna-Mochalska, M., Skrobala, A., Ryczkowski, A., Romanski, P., Piotrowski, I., Kulcenty, K., Suchorska, W.M. & Malicki, J. 2022. Nontarget and out-of-field doses from electron beam radiotherapy. *Life* 12(6): 858. https://doi.org/10.3390/life12060858

Mazonakis, M. & Damilakis, J. 2021. Out-of-field organ doses and associated risk of cancer development following radiation therapy with photons. *Physica Medica* 90: 73-82. https://doi.org/10.1016/j.ejmp.2021.09.005

Mohan, R. 2022. A review of proton therapy - Current status and future directions. *Precision Radiation Oncology* 6(2): 164-176. https://doi.org/10.1002/pro6.1149

Mohsin, N.I., Zakaria, A., Abdullah, R. & Wong, M.F. 2014. Peripheral dose measurement for 6 MV photon beam. *Journal of Medical Physics and Biophysics* 1(1): 7-9.

Momeni, N.S., Afraydoon, S., Hamzian, N., Nikfarjam, A., Ghasemabad, M.V., Dehkordi, S.A., Shabani, M., Dehastani, M. & Heldari, A. 2023. The estimation of radiation dose to out-of-field points of organs at risk in block and MLC shielded fields in lung cancer radiation therapy. *Frontiers in Biomedical Technologies* 10(2): 188-194. https://doi.org/10.18502/fbt.v10i2.12223

Naji, N.A.R., Alrubai, T.A., Ridha, A.A., Nori, W. & Najma, M.A.A. 2022. Effect of the Three Dimensional Conformal Radiotherapy (3DCRT) peripheral dose on the nipple region of the opposite breast of the obese cancer patients. *ISMSIT 2022 - 6th International Symposium on Multidisciplinary Studies and Innovative Technologies*. pp. 194-197. https://doi.org/10.1109/ISMSIT56059.2022.9932866

Oancea, C., Granja, C., Marek, L., Jakubek, J., Šolc, J., Bodenstein, E., Gantz, S., Pawelke, J. & Pivec, J. 2023. Out-of-field measurements and simulations of a proton pencil beam in a wide range of dose rates using a Timepix3 detector: Dose rate, flux and LET. *Physica Medica* 106: 102529. https://doi.org/10.1016/j.ejmp.2023.102529

Park, P.C., Zhu, X.R., Lee, A.K., Sahoo, N., Melancon, A.D., Zhang, L. & Dong, L. 2012. A beam-specific planning target volume (PTV) design for proton therapy to account for setup and range uncertainties. *International Journal of Radiation Oncology Biology Physics* 82(2): 329-336. https://doi.org/10.1016/j.ijrobp.2011.05.011

Pazzaglia, S., Eidemüller, M., Lumniczky, K., Mancuso, M., Ramadan, R., Stolarczyk, L. & Moertl, S. 2022. Out-of-field effects: Lessons learned from partial body exposure. *Radiation and Environmental Biophysics* 61(4): 485-504. https://doi.org/10.1007/s00411-022-00988-0

Podgorsak, E. 2005. *Radiation Oncology Physics: A Handbook for Teachers and Students*. International Atomic Energy Agency.

Raj, A., Khanna, D., Hridya, V.T., Padmanabhan, S. & Mohandass, P. 2022. A comparison study of out-of-field photon dosimetry between two varian linear accelerators. *Onkologia i Radioterapia* 16(9): 16-20.

Saminathan, S., Godson, H.F., Ponmalar, R., Manickam, R., Mazarello, J. & Fernandes, R. 2016. Dosimetric performance of newly developed farmer-Type ionization chamber in radiotherapy practice. *Technology in Cancer Research and Treatment* 15(6): NP113-NP120. https://doi.org/10.1177/1533034615621635

Sánchez-Nieto, B., Medina-Ascanio, K.N., Rodríguez-Mongua, J.L., Doerner, E. & Espinoza, I. 2020. Study of out-of-field dose in photon radiotherapy: A commercial treatment planning system versus measurements and Monte Carlo simulations. *Medical Physics* 47(9): 4616-4625. https://doi.org/10.1002/mp.14356

Sung, S-Y., Lee, H-Y., Tu, P-C., Lin, C-H., Yu, P-C., Lui, L.T., Shaw, S., Wu, C-J. & Nien, H-H. 2017. *In vivo* dosimetry of skin surface for breast cancer radiotherapy using intensity-modulated radiation therapy technique and helical tomotherapy. *Therapeutic Radiology and Oncology* 1: 2. https://doi.org/10.21037/tro.2017.11.01

Swanpalmer, J. 2024. Investigation of ionization chamber-specific beam quality correction factor (kQ,Q0) used for absorbed dose determination in megavoltage photon beams. *Radiation Measurements* 176: 107208. https://doi.org/10.1016/j.radmeas.2024.107208

Taylor, M. & Kron, T. 2011. Consideration of the radiation dose delivered away from the treatment field to patients in radiotherapy. *Journal of Medical Physics* 36(2): 59-71. https://doi.org/10.4103/0971-6203.79686

Technical Report Series (TRS) No. 398. 2000. *Absorbed Dose Determination in External Beam Radiotherapy.* Vienna: International Atomic Energy Agency.

Wang, K. & Tepper, J.E. 2021. Radiation therapy-associated toxicity: Etiology, management, and prevention. *CA: A Cancer Journal for Clinicians* 71(5): 437-454. https://doi.org/10.3322/caac.21689

Wiezorek, T., Georg, D., Schwedas, M., Salz, H. & Wendt, T.G. 2009. Experimental determination of peripheral photon dose components for different IMRT techniques and linear accelerators. *Zeitschrift Fur Medizinische Physik* 19(2): 120-128. https://doi.org/10.1016/j.zemedi.2009.01.008

Zhu, T.C. & Biarngard, B.E. 1994. The head-scatter factor for small field sizes. *Medical Physics* 21(1): 65-68. https://doi.org/10.1118/1.597256

*Corresponding author; email: ramacosfardela@sci.unand.ac.id